INVESTIGATION OF THE COUNTERJET DEVELOPED IN A CAVITATION BUBBLE THAT COLLAPSES NEAR A RIGID BOUNDARY

Olgert Lindau and Werner Lauterborn

Drittes Physikalisches Institut, Universität Göttingen, 37073 Göttingen, Germany

Abstract

A bubble that collapses near a rigid boundary develops a liquid jet. The jet shoots through the bubble in direction towards the boundary. When it hits the bubble wall a sequence of shock waves is emitted that is followed by the onset of a structure moving in opposite direction to the jet. This structure is called counterjet. In this paper we experimentally investigate the onset of the counterjet, the evolution of its height, the duration of its appearance and its consistence. Bubbles are induced by means of a strong laser pulse and observed with high-speed cinematography.

1 Introduction

The study of cavitation bubble dynamics near a rigid boundary has a long history and was mainly motivated by the urge to understand the destructive action on solid surfaces (see e.g. Benjamin and Ellis (1966), Lauterborn and Bolle (1975), Tomita and Shima (1986) and references therein). In the meantime many different aspects of bubble dynamics have been observed. In this paper the counterjet is investigated.

During collapse in the vicinity of a boundary a bubble develops a liquid jet. The jet shoots through the bubble with a high velocity and initiates a counterjet when it hits the bubble wall. The counterjet emerges very fast and grows in opposite direction to the jet (see figure 1). It stays visible for a long time. Even though it can be found in older recordings (see e.g. Harrison (1952) or Kling and Hammitt (1972)) the first description of the counterjet is from Lauterborn (1974).

The counterjet is a peculiar entity. Its origin is not yet known with certainty. In fluid dynamic simulations (e.g. Blake, Keen, Tong and Wilson (1999)) a counterjet does not appear. However, its appearance stays an experimental fact as it can also be found in many relatively recent publications (see e.g. Tomita and Shima (1986), Vogel, Lauterborn and Timm (1989), Ward and Emmony (1991) and Philipp and Lauterborn (1998)). This discrepancy between experiment and numerical simulations leads to the assumption that the counterjet is not an actual part of the bubble but is created in the liquid by some other mechanism during bubble collapse. It consists apparently of cavitation (micro) bubbles. As detailed in the discussion section it is very likely that the counterjet emerges in the tail of a toroidal shock wave that forms during the rather complicated collapse dynamics near the bubble minimum.

2 Experiment

In the experiment bubbles are generated with a strong laser pulse and observed with high-speed cinematography. The experimental setup is shown in figure 2.

A Q-switched Nd:YAG laser delivers single laser pulses of 8 ns width and up to 780 mJ energy at a wavelength of 1064 nm and repetition rate of 1 Hz. The laser beam is attenuated by infrared filters and focused with an aberration minimized lens system into a cuvette filled with clean, distilled water. A rigid boundary is placed below the bubble. The dimension-less distance

$$\gamma = \frac{s}{R_{max}},$$

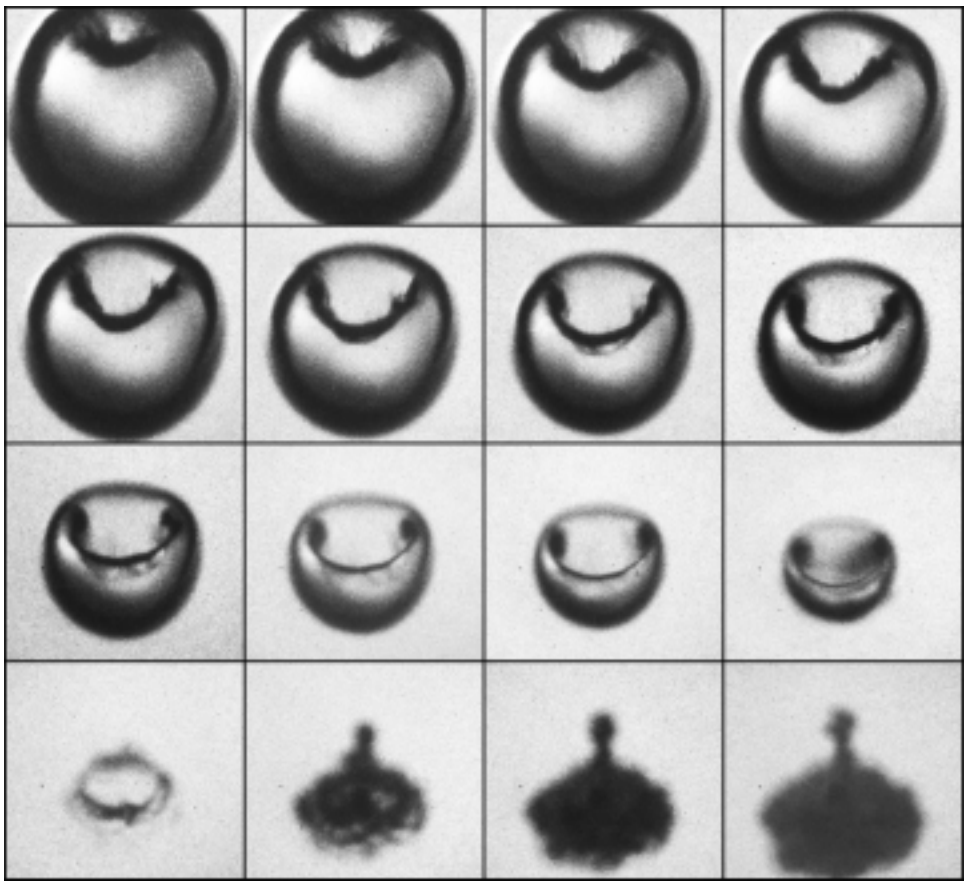

Figure 1: Jet and counterjet development in 45° view towards the boundary. Interframe time 1 μs, exposure time 200 ns, $\gamma = 2.6$, $R_{max} = 1.5$ mm, frame size 1.2 mm $\times$ 1.1 mm.

where s is the distance of the boundary from the bubble center and R_{max} the maximum bubble radius, serves as asphericity parameter. The time t_{12} between shock wave emission at bubble generation and in the first minimum after collapse is recorded with a hydrophone. The period of time t_c between the first bubble maximum and the subsequent minimum is called collapse time and equals $t_{12}/2$. Bubble size (R_{max}) can be calculated using Rayleigh's formula (Rayleigh (1917))

$$R_{max} = 1.09 \sqrt{\frac{p - p_v}{\rho}}\, t_c^*,$$

where p is the ambient, p_v the vapour pressure and ρ the density of the liquid. Here t_c^* is a modified collapse time: $t_c^* = t_c/k_1$, altered by the γ-dependent parameter $k_1 \geq 1$ given by Vogel and Lauterborn (1988). The time t_{12} and thereby R_{max} is controlled via the laser energy.

To study the onset of the counterjet, an high-speed camera (Imacon 468, Hadland) is used. In the camera the incoming light is divided into eight separate optical paths. Using eight ICCD modules that are individually triggered by a 100 MHz delay generator a high time resolution (up to 10 ns) can be achieved. A long distance microscope (QM 100, Questar) is placed in front of the camera giving a resolution of about 3 μm/pixel. A bright xenon flash is used for illumination of the sequences shown in figures 1 and 3 and a photo flash (Metz 36 CT 2) for figures 6 and 7.

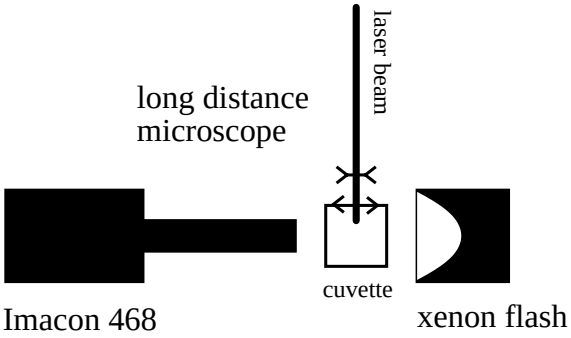

Figure 2: Experimental setup for bubble generation and observation with high-speed cinematography (top view).

3 Results of counterjet observation

The development of the jet during collapse and the onset of the counterjet are shown in figure 1. In the first frame of the sequence the bubble is almost spherical. It has a smooth surface and displays an inwardy directed dent on top (opposite to the boundary). In this frame the bubble has a radius of 0.6 mm and its volume has contracted to 6% of the bubble volume in the maximum. In the following frames, as the collapse progresses, the bubble volume shrinks further. The dent widens and forms a liquid jet that penetrates into the bubble in direction towards the boundary. Shortly before the first frame of the 4th row the jet has hit the lower bubble wall. The bubble now has the shape of a thin ring. In the second frame of the 4th row the bubble is in rebound. A counterjet has developed and is visible on top of the bubble. It is not discernible whether bubble and counterjet are connected or not. In the following frames bubble and counterjet grow in size. Both, bubble and counterjet, show a rough surface and are opaque.

In previous work it has been shown that a counterjet develops only for $3 \gtrsim \gamma > 1$ (Vogel, Lauterborn and Timm (1989)). This finding is confirmed in the present study. The counterjet appearance is coupled to the location of jet impingement. It only emerges when the jet strongly hits the bubble wall during collapse. For high values of γ the jet impact on the bubble wall becomes weak or does not happen. For $\gamma \leq 1$ the bubble begins touching the boundary during expansion and bubble dynamics changes significantly. The jet then directly impinges on the boundary, the bubble shape during collapse becomes toroidal and no counterjet is formed.

3.1 Formation velocity

A systematic investigation is undertaken to quantify the formation velocity of the counterjet. Therefore γ is varied and the first 8 μs of the counterjet onset are filmed in side view.

Figure 3 shows four sequences of the counterjet formation for $\gamma = 2.6$, 2.2, 1.8 and 1.4. In the first frame of each row the bubble is seen shortly after the emission of shock waves during bubble collapse. Beginning with the second frame the counterjet becomes visible. In the following frames it grows in width and height and the maximum counterjet size increases as γ is decreased. The height of the counterjet relative to the upper bubble wall in the first frame of each row is measured. The measured values are shown in figure 4. Function (1) is fitted to the measured values and shown as lines in the figure. The graphs of the function show a very good agreement with the measurements. A discussion of the fit parameters is given below.

The evolution of counterjet height h is modeled with

$$h(t) = h_\infty \cdot \left(1 - e^{-\frac{t-t_0}{\tau_1}}\right) + v_a \cdot (t - t_0), \quad t \geq t_0. \tag{1}$$

This function has two terms. The first term describes a growth to a maximum height h_∞. The counterjet emerges at $t = t_0$ and at $t - t_0 = 2.3 \cdot \tau_1$ its height is $h = 0.9 \cdot h_\infty$. The second term adds a constant growth with the velocity v_a. In this description the counterjet height $h(t)$ eventually exceeds h_∞ for high values of t. Its velocity starts with $h_\infty/\tau_1 + v_a$ and diverges to v_a as $t \to \infty$.

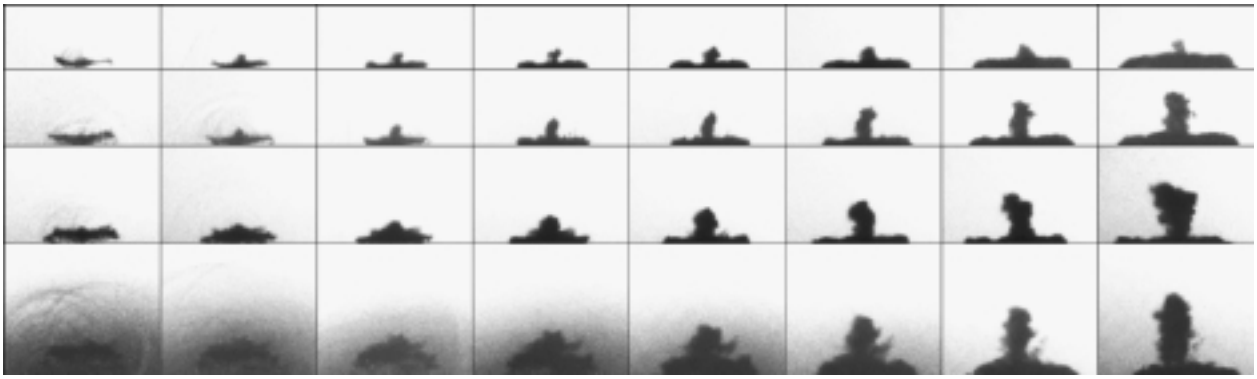

Figure 3: Onset of the counterjet for $\gamma = 2.6$, 2.2, 1.8 and 1.4 in side view (top to bottom) 10, 120, 250, 500, 1000, 2000, 4000 and 8000 ns after shock wave emission in collapse (left to right). Exposure time 10 ns, $R_{max} = 1.5$ mm, frame width 1.16 mm.

The graphs of the function (1) show a very good agreement with the measured values (see figure 4). The parameter t_0 is in the order of few nanoseconds. This is expected since the first frames of figure 3 approximately show the beginning of the counterjet onset. The linear growth velocity v_a is almost independent of γ and has a mean value of $\langle v_a \rangle = 16(5)$ m/s. The γ-dependence of h_∞ and τ_1 is shown in figure 5. The reduced counterjet height h_∞ is 100 μm at $\gamma = 2.6$ and doubles for $\gamma = 1.4$. The time parameter τ_1 equals 170 ns at $\gamma = 2.6$ and increases about ten times as γ is reduced to 1.4. This means that by decreasing γ the formation velocity of the counterjet reduces while its height eventually becomes larger.

3.2 Duration of appearance

In this subsection the counterjet evolution is investigated over a longer period of time. The observation period is 1.1 ms and two orders of magnitude longer than in section 3.1. In figure 6 six sequences of the counterjet evolution are shown. The asphericity parameter is $\gamma = 2.6$, 2.2, 1.8, 1.6, 1.4 and 1.2 from top to bottom. The interframe time increases from frame to frame and the exposure time is 30 ns. The first frame of each sequence shows the counterjet about 5 μs after its onset.

For $\gamma = 2.6$ the counterjet has vanished 50 μs after its onset. This is because in the rebound the bubble grows over the counterjet (see 2nd frame, 1st row). The counterjet for $\gamma = 2.2$ has become large enough that it survives the rebound of the bubble. Its intensity decreases in time and 100 μs after its onset it its visibility has become poor (see 3rd frame, 2nd row).

For lower values of γ the counterjet remains visible over the whole period of observation. As γ is decreased its height increases and its growth velocity becomes slower. For $\gamma = 1.4$ (5th row) this velocity is 6.7 m/s between the first two frames and 1.7 m/s between the second and third frame. Thereafter it becomes less than 0.5 m/s. This is much less than the velocity v_a specified in the last subsection. This means that function (1) loses its validity on longer time scales. Modification of the second term ($v_a \cdot (t - t_0) \rightarrow \tau_2 v_a \cdot (1 - \exp(-(t - t_0)/\tau_2))$) yields

$$h(t) = h_{max} - h_\infty e^{-\frac{t-t_0}{\tau_1}} - (h_{max} - h_\infty) \cdot e^{-\frac{t-t_0}{\tau_2}}. \qquad (2)$$

Here two new parameters have been introduced. The first parameter h_{max} is a combined factor equal to the maximum counterjet height: $h_{max} = h_\infty + \tau_2 v_a$. The second parameter τ_2 is in the order of 100 μs and depends on the value of γ. The function (2) properly describes the height until about 1 ms after counterjet onset. On longer time scales buoyancy becomes important and a third term has to be added to correctly describe the height of the counterjet.

3.3 Consistence

Shortly after its onset the counterjet appears dull and opaque (see e.g. figure 6, 1st column). Its consistence seems to be similar to that of a bubble during rebound. In contrast to the bubble its appearance modifies

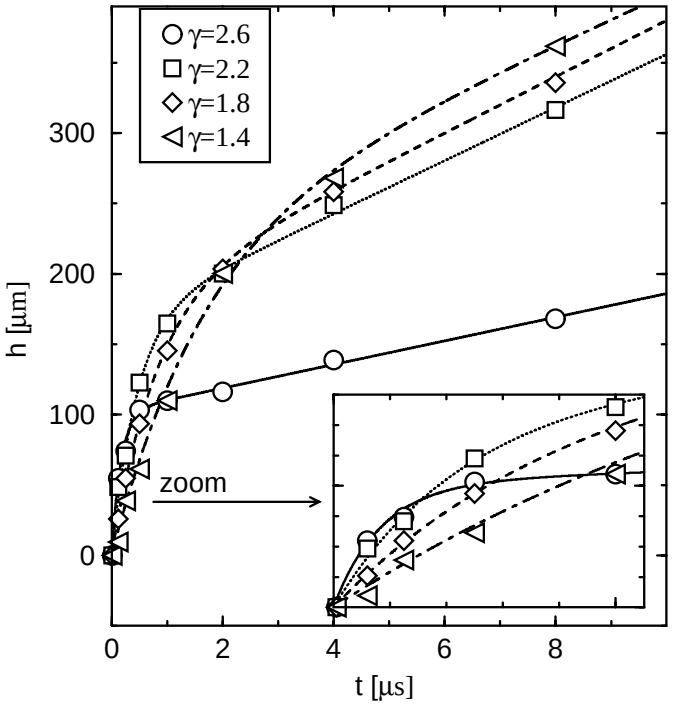

Figure 4: Counterjet height in dependence of γ (the zoomed diagram displays the first 1.1 μs). Symbols show the heights measured in figure 3, the lines fits of function (1) to the measured values.

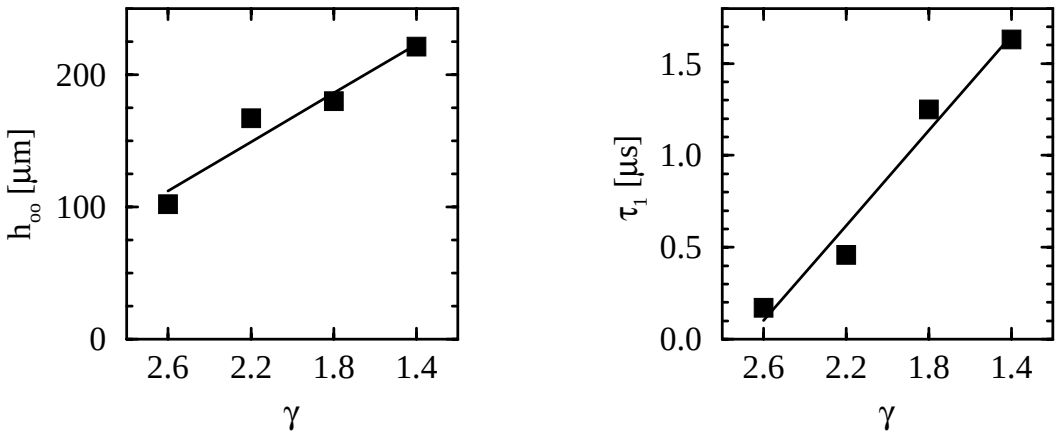

Figure 5: Values of h_∞ and τ_1 in function (1) (see text).

as the counterjet gains in size. The counterjet grows in volume while its amount of material stays the same. This means that the counterjet decays into its constituents and micro bubbles are formed. Figure 7 shows a blow up of the first four frames of figure 6 for $\gamma = 1.4$. Here the decaying process and the formation of microbubbles can be seen in detail.

4 Discussion

In the course of this study the evolution of the counterjet has been investigated both over a long observation period and in great detail with high-speed cinematography. It has been confirmed that during collapse of a

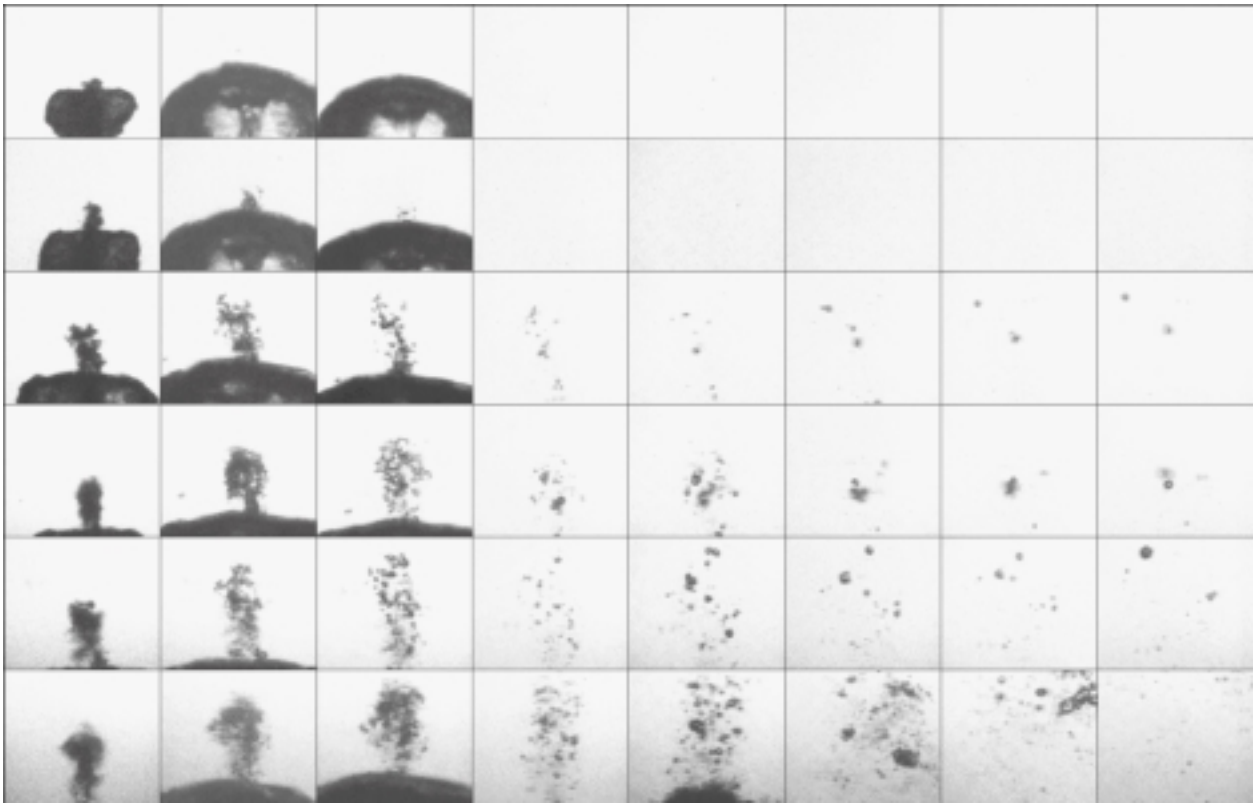

Figure 6: Evolution of the counterjet for $\gamma = 2.6, 2.2, 1.8, 1.6, 1.4$ and 1.2 in side view (top to bottom) 5, 50, 100, 200, 300, 500, 700 and 1100 μs after its onset (left to right). Exposure time 30 ns, $R_{max} = 1.5$ mm, frame size 1.42 mm $\times$ 1.21 mm.

cavitation bubble in a wide range of the dimensionless distance γ to a rigid boundary a counterjet forms. Counterjet formation is related to the impingement of the liquid jet onto the lower bubble wall. No counterjet is found for $\gamma \leq 1$ when the jet directly hits the boundary and for high values of γ when the jet impact is weak or does not happen.

It has been found that the counterjet consists of microbubbles. The evolution of its height can be described with two exponentially decaying growth rates as given in function (2). This description is valid until 1 ms after the counterjet onset. For bubbles with $R_{max} = 1.5$ mm the time parameters τ_1 and τ_2 are in the order of 500 ns and 100 μs, respectively, the maximum height h_{max} of the counterjet is in the order of 1 mm and $h_\infty \approx 150\,\mu$m. However, the parameters strongly depend on γ.

In comparison to bubble dynamics the onset of the counterjet is fast. A characteristic time for the bubble dynamics is the collapse time t_c which is in the order of 150 μs for bubbles investigated in this paper. The time τ_1 which is characteristic for the onset of the counterjet is two to three orders of magnitude shorter. This means that the counterjet is created by a fast mechanism. A possible mechanism for counterjet creation is cavitation inception that follows the self penetration of a toroidal shock wave. In the last phase of collapse a cavitation bubble emits a complicated sequence of shock waves. The first shock wave emerges on the ring where the jet hits the lower bubble wall. This shock wave indeed expands toroidally (see Lindau and Lauterborn (2000)). After the inwards moving parts meet the shock wave begins to penetrate itself in two points that move in opposite direction with high velocity. The counterjet exactly forms in the points where the shock wave penetrates itself. A very similar shock wave scenario with subsequent cavitation inception has been found at the tip of a glass fiber (Frenz, Paltauf and Schmidt-Kloiber (1996)). The glass fiber is used to deliver a short laser pulse into an absorbing liquid where a strong pressure pulse is emitted and a toroidally expanding stress wave is formed by acoustic diffraction.

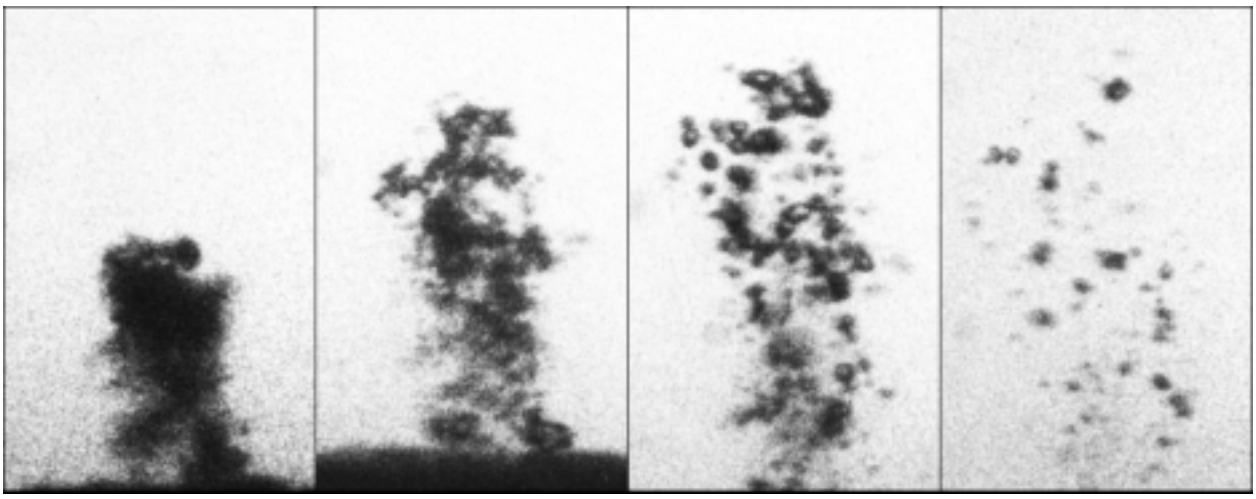

Figure 7: Evolution of the counterjet consistence 5, 50, 100 and 200 μs after its onset (part of figure 6). Exposure time 30 ns, $\gamma = 1.4$, $R_{max} = 1.5$ mm, frame size 0.77 mm $\times$ 1.21 mm.

Acknowledgment

We are grateful to the members of the Cavitation Group at the Drittes Physikalisches Institut, Göttingen, for a number of inspiring discussions. This work has been financially supported by the DFG.

References

Benjamin, T. B. and Ellis, A. T. 1966. The collapse of cavitation bubbles and the pressure thereby produced against solid boundaries. *Phil. Trans. R. Soc. London A* **260**, 221–240.

Blake, J. R., Keen, G. S., Tong, R. P. and Wilson, M. 1999. Acoustic cavitation: the fluid dynamics of non-spherical bubbles. *Phil. Trans. R. Soc. Lond. A* **357**, 251–267.

Frenz, M., Paltauf, G. and Schmidt-Kloiber, H. 1996. Laser-generated cavitation in absorbing liquid induced by acoustic diffraction. *Phys. Rev. Lett.* **76**, 3546–3549.

Harrison, M. 1952. An experimental study of single bubble cavitation noise. *J. Acoust. Soc. Am.* **24**, 776–782.

Kling, C. L., and Hammitt, F. G. 1972. A photographic study of spark-induced cavitation bubble collapse. *Journal of Basic Engineering D* **94**, 825–833.

Lauterborn, W. 1974. Kavitation durch Laserlicht. *Acustica* **31**, 52–78.

Lauterborn, W. and Bolle, H. 1975. Experimental investigations of cavitation-bubble collapse in the neighbourhood of a solid boundary. *J. Fluid Mech.* **72**, 391–399.

Lindau, O. and Lauterborn, W. 2000. Stoßwellen im Kollaps von Kavitationsblasen: Ein vertracktes Ausbreitungs-Szenario. In A. Sill, editor, *Fortschritte der Akustik (DAGA2000)*, DEGA e. V. Oldenburg, 694–695.

Philipp, A. and Lauterborn, W. 1998. Cavitation erosion by single laser-produced bubbles. *J. Fluid Mech.* **361**, 75–116.

Rayleigh, Lord. 1917. On the pressure developed in a liquid during the collapse of a spherical cavity. *Phil. Mag.* **34**, 94–98.

Tomita, Y. and Shima, A. 1986. Mechanisms of impulsive pressure generation and damage pit formation by bubble collapse. *J. Fluid Mech.* **169**, 535–564.

Vogel, A. and Lauterborn, W. 1988. Acoustic transient generation by laser-produced cavitation bubbles near solid boundaries. *J. Acoust. Soc. Am.* **84**, 719–731.

Vogel, A., Lauterborn, W. and Timm, R. 1989. Optical and acoustic investigations of the dynamics of laser-produced cavitation bubbles near a solid boundary. *J. Fluid Mech.* **206**, 209–338.

Ward, B. and Emmony, D. C. 1991. Interferometric studies of the pressure developed in a liquid during infrared-laser-induced cavitation bubble oscillation. *Infrared Phys.* **32**, 489–515.